

Dynamics and Reversible Control of the Bloch-Point Vortex Domain Wall in Short Cylindrical Magnetic Nanowires

Diego Caso¹,²,³,⁴,⁵,^{*} Pablo Tuero,¹ Javier García,¹ Konstantin Y. Guslienko^{2,3,4} and Farkhad G. Aliev^{1,5,*}


¹*Departamento Física de la Materia Condensada C03, Universidad Autónoma de Madrid, Madrid 28049, Spain*

²*Departamento Polímeros y Materiales Avanzados: Física, Química y Tecnología, Universidad del País Vasco, UPV/EHU, San Sebastián 20018, Spain*

³*EHU Quantum Center, University of the Basque Country, UPV/EHU, Leioa 48940, Spain*

⁴*IKERBASQUE, The Basque Foundation for Science, Bilbao 48009, Spain*

⁵*IFIMAC and INC, Universidad Autónoma de Madrid, Madrid 28049, Spain*

 (Received 30 September 2022; revised 18 January 2023; accepted 28 April 2023; published 8 June 2023)

Fast and efficient switching of nanomagnets is one of the main challenges in the development of future magnetic memories. We numerically investigate the evolution of static and dynamic spin-wave (SW) magnetization in short (50–400 nm in length and 120 nm in diameter) cylindrical ferromagnetic nanowires, where competing magnetization configurations of a single vortex (SV) and a Bloch-point vortex domain wall (BP-DW) can be formed. For a limited nanowire length range (between 150 and 300 nm), we demonstrate reversible transitions induced by a microwave field (forwards) and by opposite spin currents (backwards) between topologically different SV and BP-DW states. By tuning the nanowire length, the excitation frequency, the microwave pulse duration, and the spin-current value, we show that the optimum (low-power) manipulation of the BP-DW can be achieved with a microwave excitation tuned to the main SW mode for nanowire lengths around 230–250 nm, where single-vortex domain-wall magnetization reversal via nucleation and propagation of a SV-DW transition takes place. An analytical model of the dynamics of the Bloch point provides an estimate of the gyrotropic mode frequency close to that obtained via micromagnetic simulations. A practical implementation of the method in a device is proposed, involving microwave excitation and the generation of opposite spin currents via the spin-orbit torque. Our findings open up an alternative pathway for the creation of topological magnetic memories.

DOI: [10.1103/PhysRevApplied.19.064030](https://doi.org/10.1103/PhysRevApplied.19.064030)

I. INTRODUCTION

In the last few decades, numerous advances have been made in the development of spin-based data-storage and information-processing devices. Low-dimensional structures with a confined magnetic vortex have been in focus as a promising candidate for the creation of novel types of quantum magnetic memories. Their functionality as magnetic memories is based on control of a change in their topology, mainly between two distinct magnetization configurations. For example, control of the polarity of magnetic vortices created in nanometric disks (i.e., with functionality primarily restricted to the material plane [1]) through the excitation of spin waves (SWs) [2–4] has been demonstrated. A great advantage of using the excitation of SWs compared with using the spin transfer torque (STT) [5], spin-orbit torque (SOT) [6], or a magnetic field [7] for topology control is the possibility of fine control of the

topology of each individual element by tuning the excitation frequency. So far, the most widely used method to drive domain walls (DWs) locally has been by the injection of spin currents [8,9].

The emerging three-dimensional (3D) magnetic structures [10] allow a greater variety of textures and magnetic topologies to be achieved, leading to new effects [11,12]. An example of this is the creation of tunnels of chiral “skyrmions” and “bobbers,” which are more complex 3D magnetic textures in nanoribbons [13]. Topological singularities such as Bloch points (BPs) [14] have been recently found to play a critical role in 3D magnetic textures hosting skyrmions [15] and hopfions [16,17]. 3D magnetic textures are of special interest in the context of magnetic media because the employment of 3D magnetic topological solitons such as hopfions, DWs, and BPs can open up a route to creating new kinds of magnetic information-storage and spintronic devices based on 3D architectures.

Ferromagnetic (FM) nanowires (NWs) are simple systems for confining and exploring 3D magnetism that have

*farkhad.aliev@uam.es

attracted considerable attention over the last few decades. Cylindrical nanowires (having typical radii of 30–60 nm) made of ferromagnetic materials have been proposed as an alternative material for the development of numerous electronic and spintronic devices. Nanowires have robust microwave (MW) absorption [18], whose frequencies can be adjusted over a wide range depending on the choice of FM material, which is ideal for the production of MW devices

One of the most studied potential applications of ferromagnetic NWs is the development of magnetic memories. The possibility of arranging them in hexagonal arrays of high density [19] makes them excellent candidates for this type of device, since they allow high information-storage densities to be reached. Also, their shape allows the creation of vortex-type flux-closure magnetic textures [20, 21], which reduce the magnetostatic interaction between the NWs. Specifically, the possibility of creating magnetic memories based on DWs has been studied [8,9], having been inspired by a proposal for racetrack memories [22] based on the storage of information in the form of DWs displaced by pulsed electrical currents.

Although the static properties of long cylindrical nanowires have been well studied in recent years [20,23], with some indications of the possibility of magnetization reversal via a BP singularity inside a vortex DW [24], investigations of the statics and, especially, the magnetization dynamics of short NWs, where DWs and BPs emerge, are absent.

BPs were first studied and named by Feldtkeller [14], and consist in exchange-dominated 3D magnetic textures that hide topological singularities with the defining property that around them every magnetization orientation is present only one time. BP-DWs, therefore, are complex 3D textures, composed of two facing magnetic vortices with head-to-head or tail-to-tail vortex cores that might normally appear in thick NWs, where the DW magnetization is allowed to curl around the NW axis, minimizing the magnetostatic energy [25]. The dynamics of BP-DWs has been investigated only in relatively long NWs (with a wire length of about 10 times the diameter), where the BP is stabilized via bamboolike shapes [26,27].

In this paper, through micromagnetic simulations and analytic theory, we carry out a detailed investigation of BP-DW dynamics in relatively short (with a length of up to 3 times the diameter) cylindrical NWs, where a transition between a single-vortex (SV) and a vortex DW state confining a BP takes place. We also investigate the influence of pinning on the stability of the BP. Finally, we suggest a device that uses MWs and the SOT to control a transition between two different magnetic configurations, aimed at the creation of a topological magnetic memory based on short cylindrical NWs with fine frequency tuning and a latency time below 1 ns, i.e., similar to that observed using

the combined impact of SOT, STT, and voltage control of the magnetic anisotropy [28].

II. METHODS

A. Simulation details

Micromagnetic simulations are carried out using the open-source software package MuMax3 [29]. The discretization cell size is set to $1.5 \text{ nm} \times 1.5 \text{ nm} \times 1.25 \text{ nm}$, much below the exchange length, which is approximately 3 nm for $\text{Fe}_{28}\text{Co}_{67}\text{Cu}_5$ (hereafter referred to as the Fe-Co-Cu nanowire) [26], the material selected for our NWs. The cell size is chosen based on the spatial scale of the magnetic topological textures that can appear in the system. We estimate a DW and vortex-core thickness of about 10 nm. The NW diameter is set to 120 nm, and its length is varied between 50 and 800 nm (for statics) and between 50 and 400 nm (for dynamics). Previously studied NWs were mainly either much longer (more than $1 \mu\text{m}$ in length) or almost disk-shaped (circular dots with a thickness much less than 100 nm). We use typical magnetic parameters of ferromagnetic Fe-Co-Cu NWs in our simulations [24]: $M_s = 2 \text{ T}$, $A_{\text{ex}} = 25 \times 10^{-12} \text{ J/m}$, $\alpha = 0.01$, where M_s is the saturation magnetization of the NW, and A_{ex} and α describe the exchange stiffness constant and the damping of the NW, respectively. α is reduced to 10^{-4} in the dynamic simulations to better resolve the modes of the system. For the purposes of simplicity and future reference in this study, we take the NW axis to be parallel to the z axis in a Cartesian coordinate system [see Fig. 1(a)], i.e., the base of the NW is placed parallel to the x - y plane. Because of their cylindrical geometry, the NWs display a considerable shape anisotropy of magnetostatic origin, which favors a magnetization that is aligned with the direction of the NW axis. No additional magnetocrystalline anisotropies are introduced in our simulations.

In order to reveal the main SW modes, the average in-plane magnetization of the system is analyzed by means of a Fourier transform [30] to the frequency domain after the application of a homogeneous magnetic field pulse in the following form:

$$\mathbf{H}_{\text{pulse}} = H_{\text{pulse}} \text{sinc}\left(\frac{2\pi t}{t_0}\right) \hat{\mathbf{u}}_y, \quad (1)$$

where H_{pulse} is the amplitude of the applied field pulse, 2 mT, and t_0 is the full width at half maximum of the pulse, $1 \times 10^{-12} \text{ s}$. The linearity of the excited SW modes is checked up to a field magnitude of 10 mT, well above the field amplitude used. The function used for the pulse is $\text{sinc}(x) = \sin(x)/x$, which gives better results than a Gaussian function, allowing us to obtain narrower and better-defined peaks in the spin-wave excitation spectrum given by the Fourier transform.

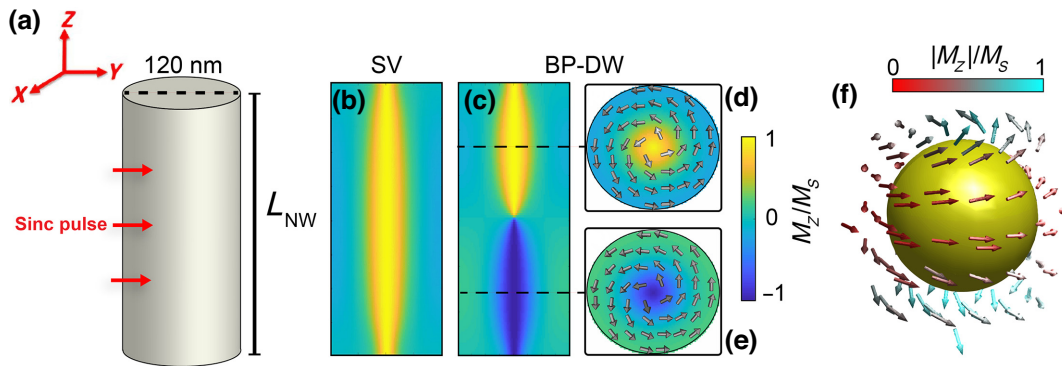


FIG. 1. (a) Sketch of a cylindrical nanowire and its orientation with respect to Cartesian coordinate axes, showing the direction of the microwave magnetic field sinc pulse applied to excite the spin eigenmodes of the system. (b),(c) Vertical sections (x - z plane) of a 250-nm-long nanowire showing a SV (b) and a BP-DW (c) magnetization configuration with a vortexlike BP-DW in the middle. The arrows illustrate the in-plane magnetization, and the colors are an indication of the out-of-plane magnetization. (d),(e) Transverse sections (x - y plane) of the nanowire in the BP-DW state are shown for the planes $z = 3L_{\text{NW}}/4$ (d) and $z = L_{\text{NW}}/4$, (e) (see dashed lines in (c)). The two vortex domains display opposite vortex polarities. (f) Three-dimensional magnetization configuration surrounding a BP-DW centered on the middle of a 250-nm-long nanowire. The colors represent the magnitude of the axially aligned magnetization.

III. NUMERICAL RESULTS AND DISCUSSION

We analyze the simulation results in this section. First, the static magnetic configurations and the related energies of NWs without induced pinning are investigated as a function of the NW length. Then, we investigate the main spin-wave modes (in both SV and BP-DW states) and their evolution with the length of the NW. Finally, ways of performing transitions between configurations with different topologies (i.e., SV versus BP-DW) are presented.

A. Static magnetization

Depending on the NW length and on the initial static magnetization configuration (ordered or disordered), the relaxation of the NW can potentially result in different stable states. If the final states correspond to a local minimum of the total magnetic energy, this means that a relatively small excitation could make the system evolve into a neighboring ground state. In other words, when a system has metastable states that are topologically different but closely situated in energy, a relatively small excitation of the spin-wave eigenmodes (involving small microwave power) may trigger a transition between two states. We therefore introduce an analysis of the possible static magnetization configurations, together with their related energies.

Figure 1(b) shows a vortex state formed after relaxing a 250-nm-long NW from a SV configuration, while Fig. 1(c) exhibits a BP-DW created after relaxing an initial configuration of two vortices with opposite polarities, one in each half of the nanowire [a front view of each vortex can be seen in Figs. 1(d) and 1(e)]. Although the resulting BP-DW state is found to be stable (within reasonable simulation conditions of torque minimization [29]), it is well known

that, in practice, metastable states (such as for example a double-vortex state [4]) are stabilized by the unavoidable natural pinning. We analyze the effect of induced pinning on the stabilization of the BP-DW state in Appendix D.

Our paper concentrates mainly on intermediate-length NWs (100–400 nm in length and with an aspect ratio between approximately 1 and 3), whose static and dynamic responses have not been covered in the literature. The typical cylindrical nanowires or dots investigated previously either were much longer (with a length greater than or equal to 1 μm), and multiple DWs [19,21] were created along their length when relaxed, or were shorter (with a length approximately equal to the radius), approaching a disk geometry where only the singular vortex state can be stabilized [2,3]. Figure 2(a) shows the energy densities for both magnetic configurations for NW lengths between 70 and 800 nm. Below 70 nm, the BP-DW state is not as stable, as it repeatedly falls into the SV state due to the magnetostatic energy of the NW, so that the situation becomes closer to resembling that of a disk under those conditions.

The energy of each configuration is found to be much lower than the magnetic energy of a saturated nanowire with a saturation magnetization parallel to the NW axis [see Fig. 2(b)], reinforcing the idea of a system with two energy-proximate states, which could show transitions from one state to the other with a given excitation.

Figure 2(a) shows the difference between the energies of one (SV) and another (BP-DW) inhomogeneous magnetization state of interest [i.e., $\Delta E = E(\text{BP-DW}) - E(\text{SV})$]. The energy difference between these states is approximately equal to 5% of the total energy value. Therefore, these NW lengths seem to be suitable for transitions between single-vortex and BP-DW states induced by external stimuli, since the two states have similar energies

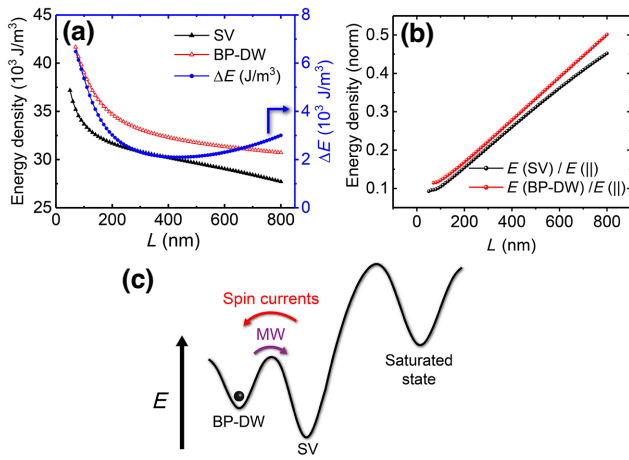


FIG. 2. (a) Total energy density of both magnetic configurations studied (SV and BP-DW) for NWs with lengths between 70 and 800 nm, and the gap [$\Delta E = E(\text{BP-DW}) - E(\text{SV})$] between them, shown in blue. (b) Energy density of the SV and BP-DW states for NWs with lengths between 70 and 800 nm normalized to the parallel saturated state. (c) Sketch of the two-level (BP-DW and SV) system and transitions that exist in NWs in the length range studied (100–400 nm).

[see Fig. 2(c)]. This difference initially decreases with increasing length, favoring the formation of DWs for longer NWs and single-vortex states for shorter ones. However, it starts increasing for NWs longer than 450–500 nm, showing a minimum in the range from 250 to 450 nm.

Therefore, we can assume that the most efficient SV-BP transitions may occur in this length range. For the longest NWs, we observe that the formation of two BP-DW states inside the NW reduces the energy with respect to a single BP-DW state, explaining the origin of the relative increase in the energy of the BP-DW state for the longest NWs.

B. Spin-wave modes

In this part, we analyze numerically the main spin-wave modes in the SV and BP-DW states and study how a DW (and the related BP) can be displaced under the action of a MW driving field. In this study, we take advantage of the metastability of the BP-DW state in short NWs to explore the possibility of eliminating a BP-DW completely from the NW via precessional magnetization motion, using a MW excitation tuned to one of the most dominant spin-wave mode frequencies [the main mode (MM)].

As we shall see below, our method of manipulating a BP using MWs has arguments or considerations for and against, in comparison with the standard method of applying a magnetic field. The main advantage of our method is the possibility of addressing the destruction of BPs individually by tuning the external frequency, but it has the disadvantage of the need to apply opposite spin currents to restore a BP. Further below, we suggest a practical implementation of the method.

Figure 3 shows the spin-wave modes of a cylindrical NW with an initial BP-DW configuration for NW lengths

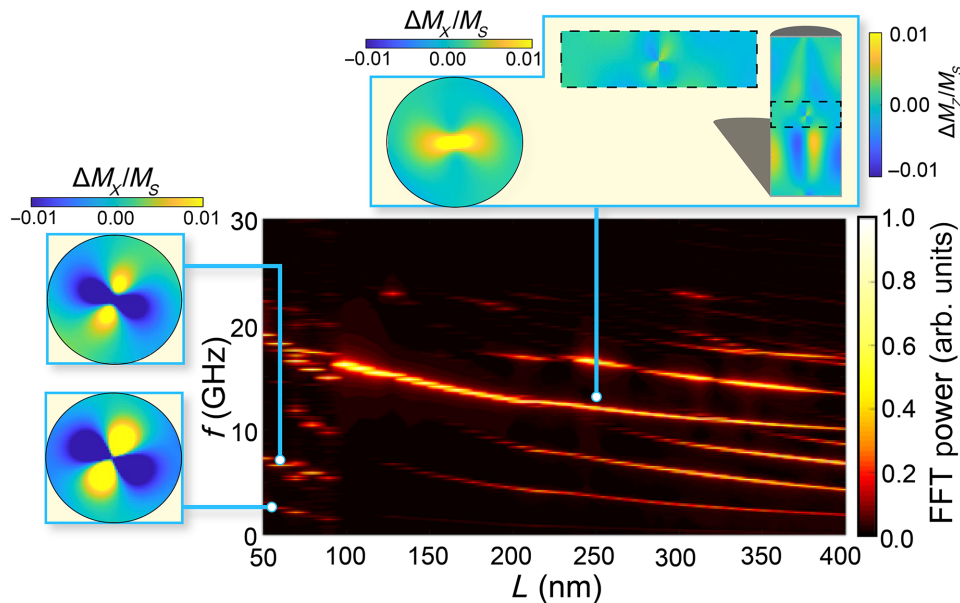


FIG. 3. Evolution of the main SW mode frequencies when the nanowire length is varied from 50 to 400 nm, obtained after relaxing the BP-DW configuration. The frequency spectra for NW lengths below 70 nm correspond to the SV state, since the BP-DW state is not stable at such small NW aspect ratios. The FFT power is normalized for each nanowire length. Snapshots of the eigenmode spatial distribution are shown for the main azimuthal modes in the SV state (where the NW length is 60 nm) and for the main mode for a length of 250 nm at the top or bottom surface of the nanowire, as well as a longitudinal cross section of the spatial distribution of the mode, focusing on the vicinity of the Bloch point (area delimited by the dashed line).

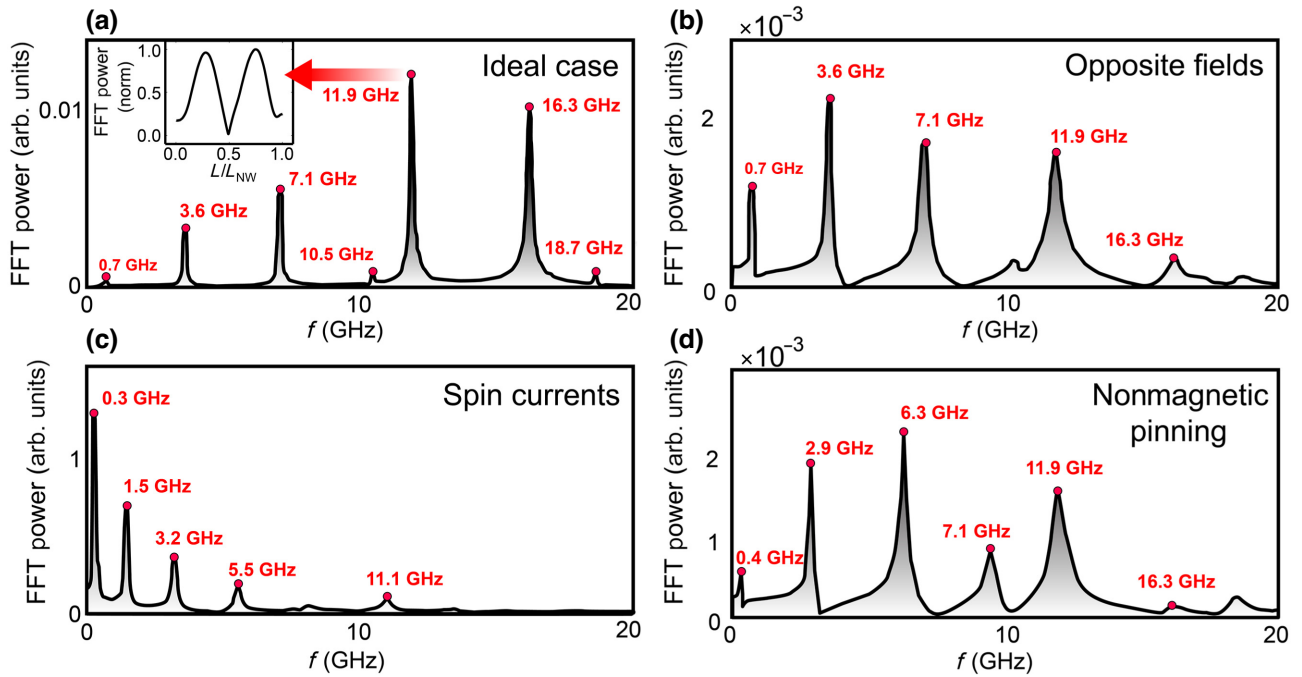


FIG. 4. Spin-wave mode spectra for a 250-nm-long NW in BP-DW magnetization configurations originating from each of the four different methods described in the text. The inset of (a) shows the normalized amplitude of the 11.9-GHz mode over the length of the NW. Videos 1 and 2 show the 11.9- and 16.3-GHz modes excited in the ideal case.

ranging from 50 to 400 nm. Even though the initial configuration is the BP-DW state, however, if the NW is short enough, this is not a stable configuration and the system relaxes into the SV state due to the magnetostatic energy contribution. This event is a direct consequence of the enhancement of the energy gap between the two states for shorter NW lengths, which makes the system no longer metastable for lengths below 70 nm. This phenomenon also translates into the dynamics of the system shown in Fig. 3: the modes detected for NW lengths below 70 nm are different in nature from those detected above 70 nm. For NWs that relax into a final BP-DW state, the frequency of the modes detected is progressively reduced as the length of the NW is increased. The SW modes are often unfolded into new modes as the nanowire length increases, providing more complicated dynamics above about 260 nm, in contrast to the simplicity of the dynamics in the range of NW lengths from 100 to 250 nm.

Figure 4 shows the calculated spin-wave modes in BP-DW configurations for a 250-nm-long NW after the BP-DW state is reached using several different protocols. What in our view are the two foremost methods (based on the ideal case and the method of spin currents) for achieving transitions between the two states investigated are described in detail in Sec. III C. Detailed explanations of the opposite-fields and nonmagnetic pinning methods are given in Appendices A and B and in Appendix D, respectively. Most of the main SW modes are present in the

majority of the reconstructed spectra. The mode located at 11.9 GHz stands out as the most prominent one when the BP-DW results from the ideal case. We find that the difference between the spectra is based fundamentally on the position of the DW, which only in the ideal case (created by hand) turns out to coincide exactly with the center of the nanowire. Furthermore, the clear fronting and tailing of the modes observed in the spectra presented in Figs. 4(b) and 4(d) are a direct consequence of the asymmetric position of the BP along the NW.

We find that BP-DW states can be effectively transformed into a SV state by MW excitation tuned to the dominant SW mode (this is referred to here as the BP-SV transition and is analyzed in detail separately). The reverse (SV-BP) transition, however, requires more detailed investigation, as the energy of the BP-DW state exceeds that of the SV configuration.

C. Creation of the BP-DW state (SV-BP transition)

We turn now to investigating in detail the SV-BP transition, using as an example a 250-nm-long NW, where the difference in the total magnetic energies between the single-vortex and DW configurations is close to the minimum [see Fig. 2(a)]. Achieving control of the SV-BP transition could be the first step in getting full control over 3D magnetization textures and their topology in short ferromagnetic nanowires.

1. BP-DW created by hand

It was detailed above how a BP-DW can be generated in the middle plane of the nanowire, with the magnetization imposed as two perfect vortex states with opposite polarities, followed by relaxation. This is achievable with the precise control of the magnetization that the simulation code provides but is challenging to carry out in practice. Because of the high symmetry that this system shows, with the BP-DW perfectly centered in the middle plane of the NW, we refer to it from now on as the “ideal” case. Figure 4(a) shows the corresponding frequency spectrum of the spin-wave modes in the ideal case, with a dominant mode at 11.9 GHz followed by a 16.3-GHz high-intensity mode. The 16.3-GHz mode seems to be relevant only in the ideal case, and has a much smaller amplitude or does not appear at all in the rest of the (less symmetric) cases considered. A detailed analysis of the modes over the NW length reveals that these modes excite mainly the vortices themselves, not the BP directly, which is what triggers BP-DW motion [see the inset of Fig. 4(a), showing the analysis of the 11.9-GHz mode].

2. BP-DW created by spin-current injection

Having verified several different ways of creating the BP-DW configuration from an initial SV state, we now concentrate on the most practical method in our view, which involves driving opposite spin currents into a ferromagnetic nanowire in order to impose the formation of the BP-DW state. In this section, we show and describe the means to create DWs in 180–300-nm nanowires using spin currents.

The application of spin-polarized currents with a polarization degree $P = 1$ in opposite directions from each of the ends of the nanowire towards its interior, with an initial magnetic configuration of a single vortex [see Fig. 5(a)], is studied in detail. The following procedure is implemented in order to evaluate the minimum spin-current density needed to successfully achieve a SV-BP transition. We allow the spin-current simulation to run for a long enough time (7 ns) to ensure the evolution of the system if the injected currents are strong enough. Then, the volume-averaged component m_z of the magnetization in the NW is evaluated over time, as it is an indication of any transitions involving the polarity of the vortex core. In a typical case of spin-current injection that leads the system to transform from a SV to a BP-DW state [see Fig. 5(d)], there are three clear regimes. First, there is an oscillation of the SV magnetization induced by the injection of the spin currents. When the oscillation becomes large enough, the SV state is no longer manifested. Two things can happen once this point is reached. If the currents are too strong, then the system does not evolve into a steady state but, rather, becomes uncontrollable; this is characterized by large and

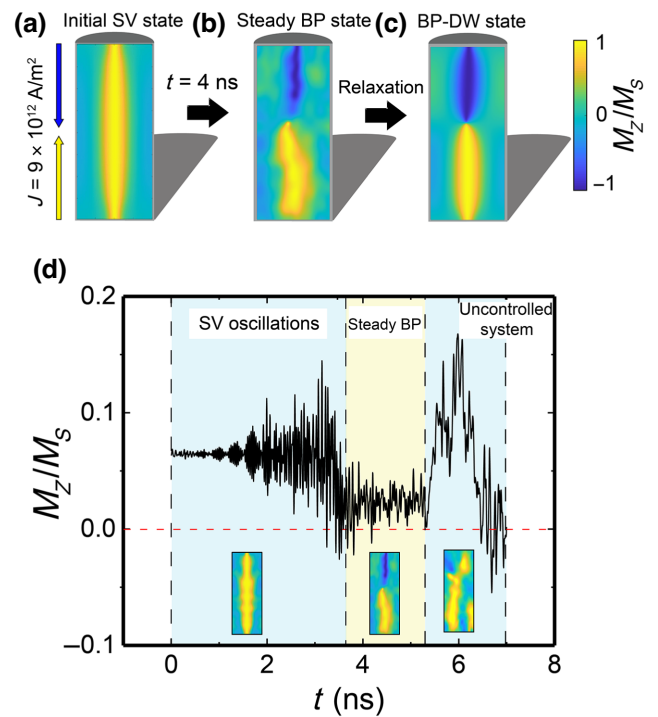


FIG. 5. Cross-section sequence of the magnetization component m_z in a 250-nm-long NW, showing the method of spin-polarized currents used to reconstruct the BP-DW state. In (a), a current of 9×10^{12} A/m² is applied in each half of the NW, in opposite directions, to the initial SV-state configuration. After 4 ns, the steady BP state is reached (b). Switching off the currents and letting the system relax returns it to the DW state (c). (d) Evolution of the average axially aligned magnetization component in a 250-nm-long NW with a spin-polarized current density of 9×10^{12} A/m². Three dynamic regimes are present in the transition. The inset images represent snapshots of the longitudinal cross section of the axial component M_z in the NW in each of the regimes. Video 3 shows the full procedure for spin-current injection in a 250-nm NW.

sharp rises and falls in the average magnetization m_z . However, if the strength of the spin currents is precisely tuned, then there is an extra step in between that displays a steady BP-DW state, before the system becomes uncontrollable [see Fig. 5(d)]. This state is manifested by a durable almost constant average out-of-plane magnetization that is close to zero.

The protocol shown in Figs. 5(a)–5(c) for obtaining a BP-DW by using spin currents is as follows. First, we apply opposite spin currents from each end of the NW towards its interior, and then the currents are removed once a steady BP-DW state is reached [see Fig. 5(b)]. By letting the nanowire relax from the steady BP-DW state, we can obtain the desired BP-DW state. Figure 5(b) shows the magnetization of the nanowire after the application of spin currents of 9×10^{12} A/m² for 4 ns, from which state the NW is relaxed to a BP-DW configuration.

Using this protocol and the appropriate current intensities, it is indeed possible to reconstruct the desired BP-DW state. For all NW lengths studied, the spin currents needed to generate a BP-DW are within the range from 9×10^{12} A/m² to 14×10^{12} A/m² [see Fig. 6(a)]. Interestingly, close to $L = 250$ nm, a minimum in the critical spin-current density J_c required to obtain the BP-DW state emerges.

Our numerical experiments reveal that the efficiency of the spin-current-induced-reversal SV-BP transition substantially increases in the vicinity of a NW length $L = 250$ nm [see the drop in the minimum spin current needed shown in Fig. 6(a)]. In order to figure out the possible origin of this unexpected behavior, we investigate the variation of the magnetization reversal modes as a function of the NW length.

Previous studies of the phase diagram of magnetization reversal modes in cylindrical NWs have shown that the reversal modes are indeed strongly dependent on the NW size [31]. The aspect ratio determines the type of DW formed [a transverse DW (T-DW) or a vortex DW (V-DW)] and the number of DWs nucleated [31]. Although the saturation magnetization used in our work is higher than that used in the work of Proenca *et al.* [31], the expected limits of the mode-reversal transition from transverse to vortex DWs should, in principle, appear for lower nanowire diameters than ours. Indeed, for the NWs with a diameter of 120 nm investigated in the present work, our simulations confirm that all magnetization reversal modes are based on V-DWs. However, the reversal modes

are quite sensitive to the length of the NW, providing variations in the presence of the different reversal modes observed even over the limited range of NW lengths studied [see the inset of Fig. 6(a)].

In particular, for the length range between 220 and 280 nm, we observe two possible reversal modes in our simulations, related to a spiral rotation of two V-DWs (2 V-DW) or, in other cases, the propagation of one V-DW (1 V-DW). Interestingly, the maximum in the probability of magnetization reversal by 1 V-DW propagation coincides with the maximum efficiency of spin-current injection [located at a nanowire length of 250 nm; see Fig. 6(a)]. We attribute this effect to a generally higher vortex symmetry in this NW length range, which matches the highly symmetric spin-current injection implemented to accomplish the backward SV-BP transition. Details of the estimation of the probability of the V-DW-mediated magnetization reversal [depicted in the inset of Fig. 6(a)] are provided in Appendix C.

D. Optimization of control of magnetization topology

In previous sections, SW modes in nanowires with BP-DW configurations have been demonstrated (Figs. 3 and 4). One can expect that these configurations, under a MW excitation at a frequency close to one of the main eigenfrequencies of the nanowire, will ultimately result in a transition between the BP-DW state (a metastable state) and the SV state (a stable state). To verify this hypothesis, a sinusoidal excitation magnetic field is applied to

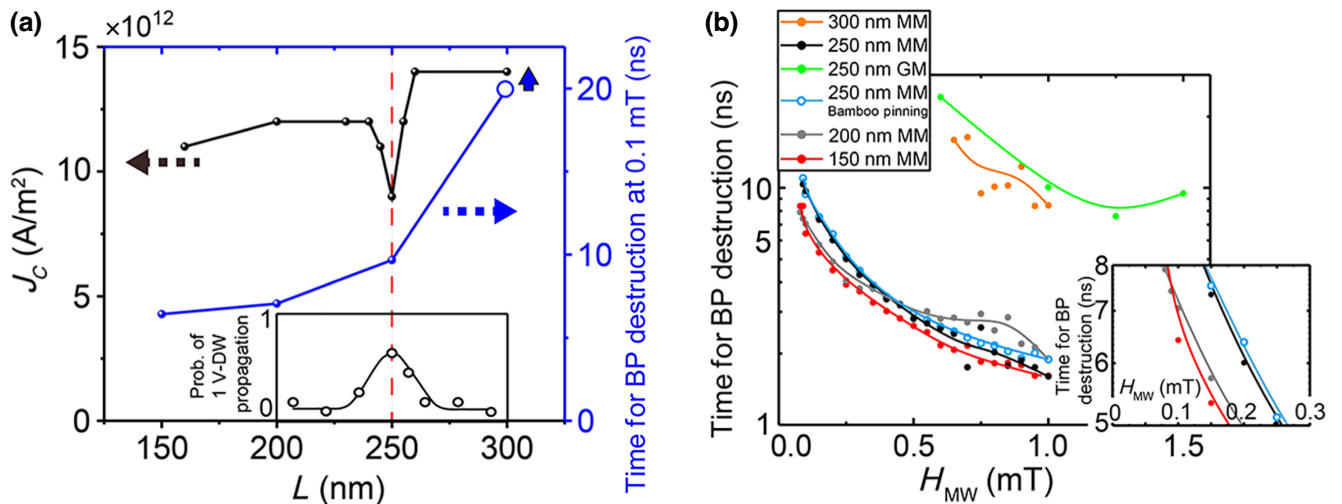


FIG. 6. (a) Critical spin-current density (J_c) needed to create a steady BP state and time for destruction of the BP-DW using the main mode at 0.1 mT, plotted as a function of the NW length. The inset of (a) depicts the probability of detecting a 1 V-DW-propagation reversal mode against the NW length. (b) Time required for the MW excitation to start to displace the DW, on a logarithmic scale, plotted against the excitation field amplitude, for different lengths of the NW. For a NW length of 250 nm, the main mode and the gyrotropic mode (GM) are studied. The inset corresponds to an enlargement of the main-mode excitations for NW lengths ranging from 150 to 250 nm. The point at 300 nm in the curve of the time for destruction in (a) is a lower-end estimate following the trend in (b). Video 4 shows the transition from the BP-DW state to the SV state under the application of a MW excitation field matching the frequency of the main SW mode in a 250-nm NW.

each magnetization configuration as follows: $\mathbf{H}_{\text{excitation}} = H_{\text{MW}} \sin(2\pi ft) \hat{\mathbf{u}}_y$, where H_{MW} is the excitation amplitude and f is the frequency of the SW mode used to excite the NW. The MW field applied throughout the whole NW is directed perpendicular to the NW axis, similarly to the sinc pulse used before to demonstrate the SW eigenmodes of the system [see Fig. 1(a)].

The result of applying the MW field is as follows: after a certain time (which depends on the intensity of the excitation and the SW mode frequency used), the BP-DW moves towards one of the two ends of the NW and a SV state is created in the NW. Figure 6(b) shows the dependence of the time of application of the MW excitation required to remove the BP-DW as a function of the excitation amplitude for different NW lengths. The 11.9-GHz mode is chosen as the main SW mode for this study, since it is notably present in all SW excitation spectra shown in Fig. 4. The time for destruction becomes effectively larger if the excited SW mode is not the main one in terms of amplitude. For example, if the 250-nm BP-DW nanowire is excited at a frequency close to the frequency of its gyrotropic mode (located at 0.69 GHz for a 250-nm NW length), which is directly related to oscillations of the BP position and should induce a more localized excitation of this magnetization texture, then the time for BP-DW destruction becomes much larger [see Fig. 6(b)], even though, over time, the transition is eventually accomplished. Latency times below 1 ns are accomplished in our system by exciting the most predominant SW mode (11.9 GHz) with MW fields exceeding 5 mT (see Appendix E).

Figure 6(b) shows that the transition from the BP-DW to the SV state takes longer to occur as the amplitude of excitation decreases. For MW excitation amplitudes smaller than those shown, displacement of the DW is not observed for times below 10 ns. It can be seen that the transition occurs for relatively short times even with small MW field amplitudes (approximately 0.2 mT). Figure 6(b) also shows a big leap in the efficiency of BP-DW destruction when the NW length is changed from 250 to 300 nm. This effect may be attributed to a transition from a regime in which several SW modes of similar amplitude are involved in the dynamics of the system, for 300-nm-long NWs, as opposed to a regime in which the dynamics relies on one dominant main mode, for 250-nm and shorter NWs (see Fig. 3). This recipe, therefore, presents a way of moving domain walls in a nanowire with a relatively small energy cost. The BP velocities in the destruction process reach approximately 400 m/s, and such high velocities are observed even with a small applied field.

Figure 6(a) compares the time required to remove the BP-DW using a MW excitation of 0.1 mT at the frequency of the main SW mode and the minimum spin current required to restore the BP-DW, in the NW length range where such reversible transitions are found to be possible to perform. The energy required for the BP-DW

destruction-and-restoration cycle can be obtained from these two graphs. Simulations suggest that the time needed for BP-DW destruction increases notably in the NW length range from 250 to 300 nm due to topological differences arising from the fact that a single BP-DW is more stable for lengths in this range [see Fig. 6(b)]. However, for NW lengths from 150 to 250 nm, the time for destruction is almost constant. The reconstruction with spin currents is most effective for a NW length of 250 nm, for which there is a minimum in the spin-current density J_c necessary to reconstruct the BP-DW. We conclude that the optimal length for efficiency of the SV-to-BP-DW cycle is close to 250 nm.

E. Optimization of control of the magnetization topology using the gyrotropic mode

Up to this point, the destruction of the BP-DW is performed by the application of a small MW excitation at the frequency of the main detected SW mode, 11.9 GHz. The magnitude of this mode in comparison with the others allows the destruction to be efficient both in time and in the required amplitude of the applied MW field [see Fig. 6(b)]. However, the mode spectra generated after the reconstruction of the BP-DW via spin currents display a redistribution of the mode amplitudes. Once the BP-DW state is created by injection of opposite spin currents, the gyrotropic mode becomes also the main eigenmode of the system [see Fig. 4(c)], meaning that it might be now more efficient to destroy the new BP-DW state by using the gyrotropic mode frequency as the MW excitation frequency.

Interestingly, the results obtained indicate that the effectiveness of using the gyrotropic mode to realize the BP-DW-to-SV-state transition strongly depends on the symmetry of the BP-DW with respect to the center of the nanowire. As mentioned above, to obtain a BP-DW, the injection of opposite spin currents should be stopped in the steady BP-DW regime shown in Fig. 5(d). However, even in this regime, the BP-DW does not completely resemble the configuration obtained in the ideal case, but rather is dependent on the exact moment of relaxation, resulting in a more or less symmetric outcome. As Fig. 7 shows, the time for destruction of the spin-current-reinstated BP-DW state decays as the system becomes more asymmetric. Simultaneously, the amplitude of the GM excited to accomplish the BP-DW-to-SV-state transition increases with the asymmetry of the position of the BP-DW with respect to the center of the nanowire.

IV. ANALYTICAL MODEL OF THE DYNAMICS OF THE BLOCH POINT

In order to provide an analytical estimate of the lowest (gyrotropic) spin-wave frequency in a nanowire, we consider a BP-DW in a cylindrical nanowire with a length L and radius R . We use a cylindrical coordinate system

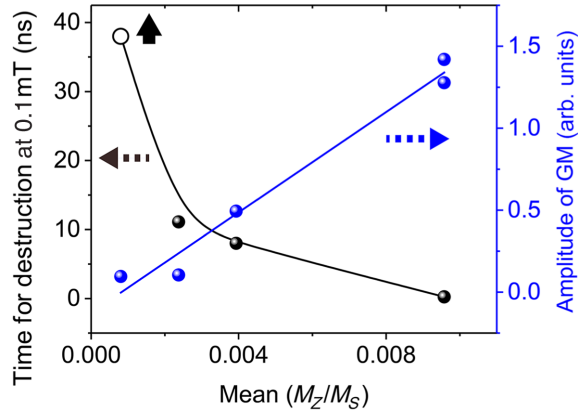


FIG. 7. Time for destruction of the BP-DW state with a MW excitation field with an amplitude of 1 mT, and the frequency of the GM and corresponding amplitude of the GM for different stopping times after the application of a spin-current density of 9×10^{12} A/m² in a 250-nm nanowire plotted against the average out-of-plane magnetization component. The point at almost 40 ns is a lower estimate of the destruction time.

(ρ, ϕ, z) with the Oz axis coinciding with the nanowire axis. We assume that the domain wall is of vortex type and that the ρ magnetization component is equal to zero, i.e., $m_\rho = 0$. We choose the magnetization component m_z to be in the azimuthally symmetric trial form suggested by Thiaville *et al.* [32],

$$m_z(\rho, z) = \frac{z}{\sqrt{\rho^2 + z^2}} \frac{b^2}{b^2 + \rho^2}, \quad (2)$$

where b is the size of the BP (of the order of 10 nm). To calculate the gyrotropic frequency of the BP excitation, we use the Landau-Lifshitz-Gilbert (LLG) equation of motion, which describes the evolution of the magnetization $\mathbf{M}(r, t)$ in a ferromagnet in the presence of an effective magnetic field \mathbf{H}_{eff} and damping. It is written in the following form:

$$\frac{d\mathbf{M}}{dt} = -\gamma \mathbf{M} \times \mathbf{H}_{\text{eff}} + \frac{\alpha}{M_s} \mathbf{M} \times \frac{d\mathbf{M}}{dt}, \quad (3)$$

where γ is the gyromagnetic ratio, α is the dimensionless damping constant, and M_s is the saturation magnetization. The effective field $\mathbf{H}_{\text{eff}} = -\delta E / \delta \mathbf{M}$ is a combination of the external magnetic field, the exchange field, and the demagnetizing field, where E is the total magnetic energy density. It was shown by Thiele [33] that for the description of the dynamics of magnetic domains, the LLG equation can be rewritten in another form that allows the calculations to be simplified. Thiele's approach is applicable to describing the dynamics of stable magnetization configurations (magnetic solitons) that can be characterized by a position of the center $\mathbf{X}(t)$ (a collective coordinate) that can vary with time. To consider the gyrotropic dynamics of a BP, we assume that the magnetization, as a function of the

coordinates $\mathbf{r} = (\rho, z)$ and time, can be written in the form $\mathbf{M}(\mathbf{r}, t) = \mathbf{M}(\mathbf{r}, \mathbf{X}(t))$. The three-dimensional vector $\mathbf{X}(t)$ represents oscillations of the center position of the Bloch point. Then, neglecting damping, we can rewrite the LLG equation as

$$G_{\alpha\beta} \frac{dX_\beta}{dt} = -\frac{\delta W}{\delta X_\alpha}, \quad (4)$$

where W is the total magnetic energy, and $\alpha, \beta = x, y, z$. Introducing the unit vector of the magnetization $\mathbf{m} = \mathbf{M}/M_s$, the components of the global (volume-averaged) gyrotensor G can be defined as follows:

$$G_{\alpha\beta} = \frac{M_s}{\gamma} \int d^3\mathbf{r} \left(\frac{\partial \mathbf{m}}{\partial X_\alpha} \times \frac{\partial \mathbf{m}}{\partial X_\beta} \right) \cdot \mathbf{m}. \quad (5)$$

The dependence of $\mathbf{M}(\mathbf{r}, \mathbf{X}(t))$ is unknown, and therefore we make the simplest assumption, that $\mathbf{M}(\mathbf{r}, \mathbf{X}(t)) = \mathbf{M}(\mathbf{r} - \mathbf{X}(t))$, which corresponds to rigid motion of the BP around the equilibrium position $\mathbf{X} = 0$. We assume that the metastable equilibrium position of the BP is located on the nanowire axis Oz at the point $z = 0$. The corresponding vortex-type DW containing this BP is located in the $z = 0$ plane, which separates the nanowire into two symmetrical domains with magnetizations directed upwards ($z > 0$) and downwards ($z < 0$). The global gyrovector given by Eq. (5) can be calculated at the BP position $\mathbf{X} = 0$ using the standard approach as

$$G_{\alpha\beta} = \frac{M_s}{\gamma} \int d^3\mathbf{r} F_{\alpha\beta}^e, \quad (6)$$

where $F_{\alpha\beta}^e = [(\partial \mathbf{m} / \partial x_\alpha) \times (\partial \mathbf{m} / \partial x_\beta)] \cdot \mathbf{m}$ is the emergent electromagnetic field tensor [34].

The tensor $G_{\alpha\beta}$ is antisymmetric and, therefore, can be represented via a dual vector \mathbf{G} , known as the gyrovector. By substituting the magnetization distribution in Eq. (2) into Eq. (6), one can calculate the components of the global gyrovector in cylindrical coordinates as $\mathbf{G} = (G_\rho, 0, 0)$. The ρ component for the case $L \gg R$ is

$$G_\rho = -4\pi b \frac{M_s}{\gamma} \text{atan} \left(\frac{R}{b} \right). \quad (7)$$

The global gyrovector is finite and is a function of the BP radius b . The equilibrium value of b can be found from minimization of the total magnetic energy of a centered BP, consisting of the exchange and magnetostatic energies. We note that nullification of the global gyrovector is a property of infinite systems with specific asymptotic behavior of the magnetization at infinity ($\mathbf{m} = \text{const}$). Such magnetization textures include localized 3D solitons and toroidal hopfions, for instance [17]. The Bloch point is a nonlocalized 3D magnetic topological soliton and may show a

TABLE I. Second derivative of the energy of a BP (in units of J/nm^2) with respect to displacements of the BP under an applied field in the transverse and axial directions in a nanowire. The simulated nanowire is 120 nm in diameter and 250 nm in length. The magnetic parameters used are $\mu_0 M_s$ (saturation magnetization) = 2 T, A_{ex} (exchange stiffness constant) = 25 pJ/m, and α (damping) = 0.01. Pinning is achieved by increasing the saturation magnetization by 2 times in the middle of the NW, where the BP is located.

	Without pinning	With pinning
Transverse displacement	1.2336×10^{-22}	2.67208×10^{-22}
Axial displacement	8.08524×10^{-20}	8.76542×10^{-19}

nonzero global gyrovector in a restricted cylindrical NW geometry, as given by Eq. (7). The finite global gyrovector allows one to calculate the gyrotropic frequency of the BP. The nonzero transverse gyrovector component (G_ρ) leads to the BP being expelled to the NW circumference for any value of the BP-DW velocity directed along the NW length, due to the gyroforce. The SV-state magnetization does not depend on the thickness coordinate z except in some small areas near the nanowire faces. Therefore, the SV state is essentially two-dimensional and described by a two-dimensional magnetic topological charge, which is proportional to the z component of the vortex gyrovector, $G_z = -2\pi L(M_s/\gamma)$. The global gyrovector of the BP-DW is a result of the more complicated 3D magnetization distribution given by Eq. (2). The ratio of the absolute values of the BP and SV gyrovectors, $G_\rho/G_z = \pi b/L$, is small for the nanowire lengths of 100–300 nm investigated in the present paper.

Accounting for the azimuthal symmetry of the system, the energy of a moving BP for small oscillations of the BP position near the equilibrium position in the center of the NW can be written as

$$W(\mathbf{X}) = W(0) + \frac{1}{2}\kappa(X^2 + Y^2) + \frac{1}{2}\kappa_z Z^2. \quad (8)$$

By solving the Thiele equation of motion, Eq. (4), for the position of the BP center $\mathbf{X}(t)$, one can find the gyrotropic oscillation frequency,

$$\omega_G = \frac{\sqrt{\kappa\kappa_z}}{G_\rho}. \quad (9)$$

The stiffness coefficients κ and κ_z are calculated numerically; see Table I. The equilibrium value of b is 7.2 nm for the given nanowire parameters. Using data from Table I and Eq. (9), one can calculate the BP gyrotropic frequency to be $\omega_G/2\pi = 0.45$ GHz without pinning and $\omega_G/2\pi = 2.20$ GHz with pinning.

V. DEVICE IMPLEMENTATION

A suitable device for implementing the proposed reversible BP-DW manipulations could include two

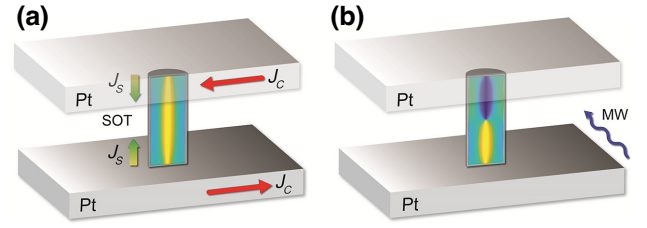


FIG. 8. Schematic illustration of the suggested device for implementing the transition mechanism described. (a) Electric current is applied simultaneously through two Pt electrodes contacting opposite ends of the NW in the SV state, triggering two opposite spin-polarized currents through the NW by the SOT, effectively switching the NW to the BP-DW state. (b) MW excitation is applied perpendicularly to the NW in the BP-DW state to trigger the transition to the SV state.

heavy-metal (Pt) electrodes located on the ends of a Fe-Co-Cu NW. These electrodes would be able to generate spin-polarized current via the SOT when an electric current is applied through the Pt, effectively restoring the BP-DW state [see Fig. 8(a)]. We note that the SOT is known to provide much higher energy efficiency and lower latency times than the STT does [35]. Additionally, the device would avoid possible heating in the NW, since the spin current and charge current are independent separate events, which would not happen with the STT.

For the BP-SV transition [see Fig. 8(b)], external frequency-tuned MWs are needed; one way to achieve this is by placing the sample on a coplanar waveguide and applying magnetic pulses. Another way is to take advantage of the two Pt electrodes and use them as a waveguide. In the latter case, the MW excitation has a predominantly axial direction. This, however, is not an issue, since we check that the BP-SV transition can indeed also be achieved using axial excitation, with similar latency times to those in the case of perpendicular MW excitation.

VI. CONCLUSIONS

In summary, we investigate numerically and by analytical theory the static and dynamic (spin-wave modes) properties of short cylindrical magnetic nanowires, where the ground (single-vortex) and metastable (with a vortex domain wall with a Bloch point) states have similar energies. We demonstrate effective reversible control of the topology of the 3D magnetization texture, which can be switched between these two states by using low-power short microwave excitation. To destroy the BP-DW state, the MW-field frequency is chosen to be close to one of the dominant SW mode frequencies. Opposite spin-polarized currents are used to reestablish the BP-DW magnetization configuration. Finally, an implementation of the mechanism in a practical device is proposed, involving the generation of opposite spin currents via the SOT. Our

results pave the way towards the creation of an alternative type of energy-efficient magnetic memory based on short ferromagnetic cylindrical nanowires.

ACKNOWLEDGMENTS

The work in Madrid was supported by the Spanish Ministry of Science and Innovation (Grants No. PID2021-124585NB-C32 and No. TED2021-130196B-C22) and the Consejería de Educación e Investigación de la Comunidad de Madrid (Grant No. NANOMAGCOST-CM Ref. P2018/NMT-4321). F.G.A. acknowledges financial support from the Spanish Ministry of Science and Innovation, through the María de Maeztu Program for Units of Excellence in R&D (Grant No. CEX2018-000805-M) and “Acción financiada por la Comunidad de Madrid en el marco del convenio plurianual con la Universidad Autónoma de Madrid en Línea 3: Excelencia para el Profesorado Universitario.” J.C. and P.T. thank the Spanish MECD and IFIMAC for support from fellowships. K.G. acknowledges support from IKERBASQUE (the Basque Foundation for Science). K.G.’s work was supported by the Spanish Ministry of Science and Innovation under Grant No. PID2019-108075RB-C33/AEI/1013039/501100011033 and by the Norwegian Financial Mechanism 2014–2021 through Project UMO-2020/37/K/ST3/02450.

APPENDIX A: BP-DW CREATED BY OPPOSITE MAGNETIC FIELDS

The first proposed method that might be experimentally achievable consists of applying two homogeneous magnetic fields in the direction of the NW axis to the vortex state, in opposite directions in each of the two halves (we call this the opposite-magnetic-fields method in what follows). If the nanowire has its main axis in the direction of the z axis and its center is at the origin of the coordinates, we can apply the following magnetic field:

$$\mathbf{H} = \begin{cases} H\hat{\mathbf{u}}_z, & z < 0, \\ -H\hat{\mathbf{u}}_z, & z > 0. \end{cases} \quad (\text{A1})$$

The protocol to be followed with this method is as follows: (i) apply the magnetic field \mathbf{H} to the nanowire, (ii) relax the nanowire in the applied field, and (iii) remove the field and relax the nanowire.

Figure 9 shows the evolution of the magnetization component m_z in the nanowire throughout these steps, which ultimately lead to the creation of a DW state from an initial SV state. This method, however, has two drawbacks. The first is the intensity of the applied magnetic field H_0 , which must be sufficient to be able to reverse the magnetization in one of the halves of the NW while maintaining that in the other half. In this case, a limiting value for the field amplitude of 0.6 T is found, below which the final state

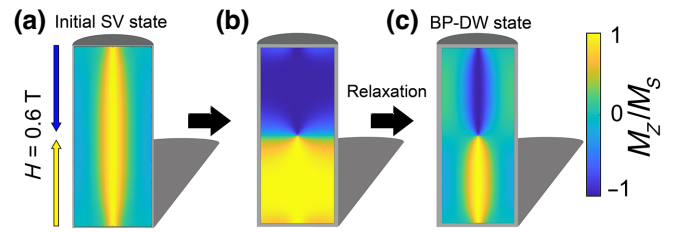


FIG. 9. Cross-section sequence of the magnetization component m_z in a 250-nm-long NW, showing the method of opposite magnetic fields used to reconstruct the BP-DW state. (a) Initial SV state before the opposite magnetic fields are applied. (b) After two 0.6-T opposite fields, the magnetization component m_z is almost completely saturated in each half of the NW. (c) After the NW is relaxed, the BP-DW state is reached.

remains a single vortex. The second drawback resides in the difficulty of creating strong magnetic fields with such a specific spatial asymmetry on a small scale.

APPENDIX B: BP-DW CREATED BY PINNING

In order to reduce the amplitude of the magnetic field necessary to create a BP-DW in the NW, the introduction of BP-DW pinning is investigated. This method is based on the addition of a defect to the system and trying to localize the BP-DW on it. In this case, a layer of nonmagnetic material is introduced into the middle plane of the nanowire [see the modes of the system in Fig. 4(d)]. Here, the same procedure is followed as in the opposite-magnetic-fields method with the exception that a nonmagnetic layer with $M_s = 0$ and a thickness of 2.5 nm is introduced in the center of the 250-nm-long nanowire. We find similar results to those for the opposite-magnetic-fields method without pinning (see Appendix A); however, the value of the critical magnetic field needed for a DW to be generated is reduced from 0.6 to 0.45 T.

Although the pinning of the BP-DW that we explore here leads us closer to the appropriate goal, it still presents drawbacks similar to those of the opposite-magnetic-fields method. One could try to reduce the critical field required to generate the BP-DW even more by adding a thicker pinning layer, but high accuracy in the symmetry of the applied opposite fields would still be needed. Besides, as we describe in Appendix D, extra pinning could complicate the goal of achieving low-energy manipulation of the magnetic SV-BP topology. We believe that the most practical way to realize the SV-BP transition is by the injection of opposite spin currents.

APPENDIX C: ESTIMATION OF THE REVERSAL MODES AND THEIR PROBABILITY CALCULATED FROM THE HYSTERESIS LOOPS OBTAINED

To obtain the data presented in the inset of Fig. 6(a), several hysteresis loops are performed, saturating at an axial

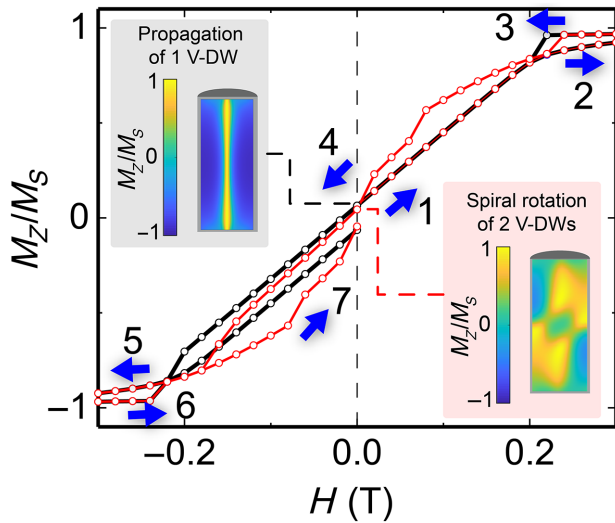


FIG. 10. Hysteresis loops for a 250-nm-long NW in the case of each of the two reversal modes presented. The insets show cross sections of the NW for two different types of detected magnetization reversal modes at $H = 0$: spiral rotation of two V-DWs (2 V-DW) and propagation of one V-DW (1 V-DW).

field of up to 1 T (see Fig. 10). At $H = 0$, when the field is being reduced, the static magnetic configuration reveals the reversal modes of the system. This process is executed for NW lengths within the range 220–280 nm, depicted in the inset of Fig. 6(a).

However, the type of reversal mode in this range is found to be uncertain, i.e., the NW hysteresis loop in an axial magnetic field is characterized by one or other particular reversal mode (either spiral rotation of two V-DWs or propagation of one V-DW) each time a hysteresis loop is performed for a specific length. This means that different reversal modes can be shown by the same system in separate hysteresis runs. This is due to the fact that the two

observed reversal modes are close in energy for most of the NW lengths studied. In order to describe the probabilistic character of the reversal-mode topology, repeated simulations of ten hysteresis loops are performed for each NW length. The inset of Fig. 6(a) represents the probability of obtaining the 1 V-DW-propagation reversal mode versus the length of the NW.

APPENDIX D: INFLUENCE OF PINNING ON CONTROL OF THE MAGNETIZATION TOPOLOGY

The BP-DW investigated is formed as a metastable state above the SV ground state (Fig. 2). This facilitates switching from the BP-DW to the SV state under a rather small fine-tuned microwave field, as well as the backward switching by using reasonable spin-current densities (Fig. 6). We investigate the efficiency of such switching not only by varying the NW length (see Fig. 6) but also through the implementation of different strategies for pinning of the BP-DW for the specific NW length of 250 nm, for which switching of the topology of the magnetic texture is found to be less energetically costly. Specifically, we introduce BP-DW pinning in such NWs by using a modulated bamboolike geometry [26,27] (geometric pinning), an enhanced local saturation magnetization M_s (magnetic pinning), or the implementation of a nonmagnetic layer (nonmagnetic pinning). We find that the energy gap between the two metastable states is reduced if pinning of the BP-DW position is introduced [see Fig. 11(a)], as a consequence of the enhanced stability of the BP-DW state under the different pinning conditions. Our simulations reveal that BP-DW stabilization is better achieved through magnetic pinning than by geometrically modulating the middle of the NW, even though the geometrical modulation is introduced in a 25-nm NW segment and the magnetic pinning is introduced in only a 2.5-nm segment.

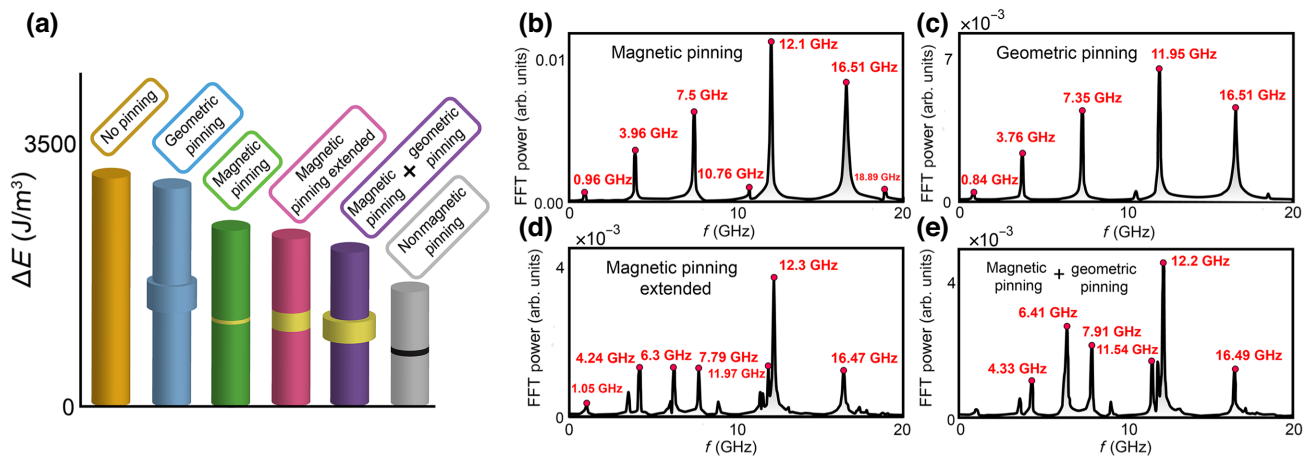


FIG. 11. (a) Energy gap between the BP-DW and the SV state for different types of pinning introduced into the NW. (b)–(e) Average spin-wave mode spectra of the different pinned systems.

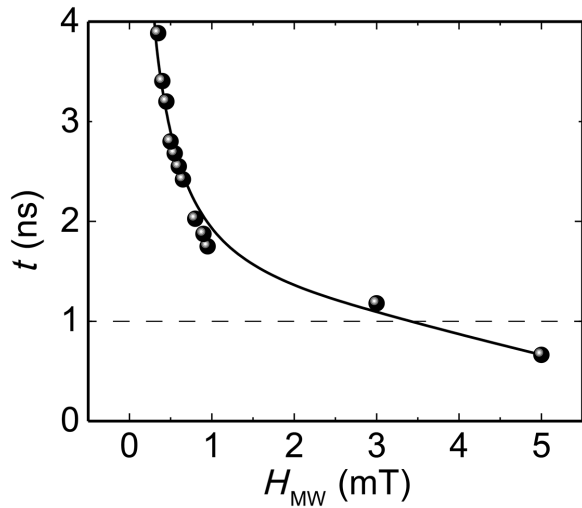
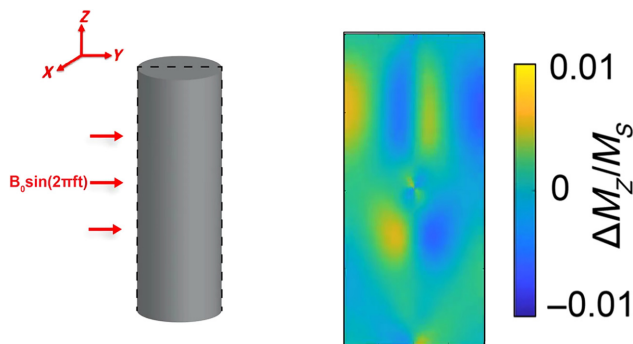


FIG. 12. Time for destruction of the BP-DW state (latency time) in a 250-nm NW under MW excitation at a frequency tuned to the main spin-wave mode observed (11.9 GHz) against the amplitude of the driving field.

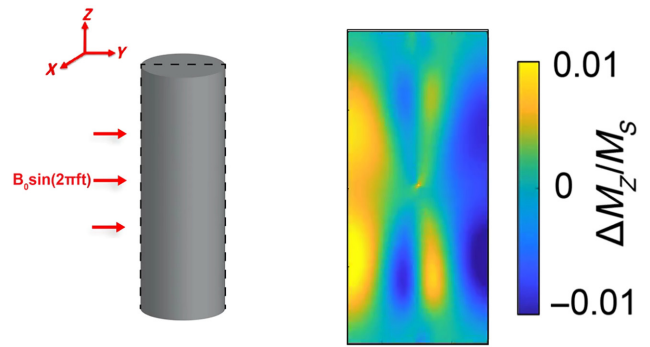
Pinning of the BP position is an additional obstacle to performing state switching via a microwave field. Thus, MW excitation of the main SW modes in the amplitude range studied (up to 2 mT) can destroy the BP-DW state only in the case of bamboolike pinning, with the times of transition being only slightly above those for an ideal-case 250-nm-long NW [see Fig. 6(b)]. For any of the other pinning methods implemented [see Fig. 11(a)], the transition from the BP-DW to the SV state is forbidden.

APPENDIX E: LATENCY TIMES IN THE HIGH-MW-EXCITATION LIMIT

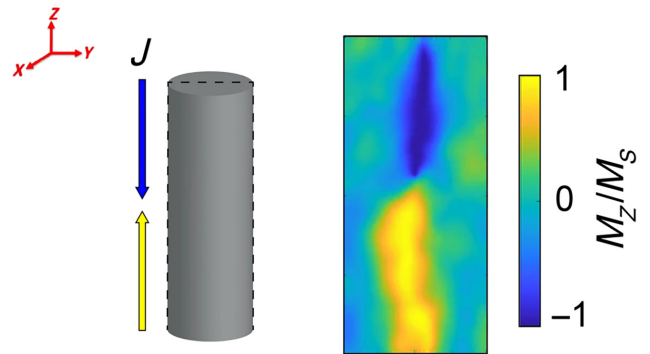
Latency times below 1 ns are achieved in the BP-DW-to-SV-state transition for high MW driving fields (see Fig. 12).



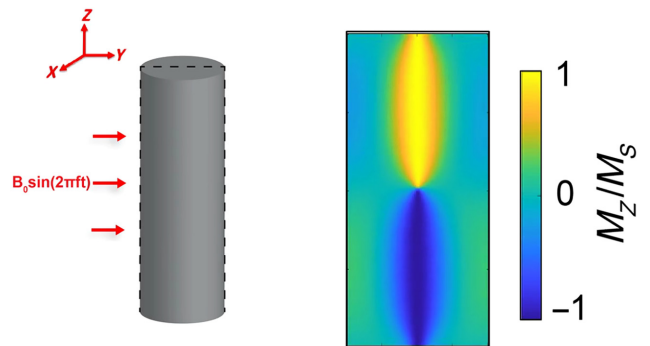
VIDEO 1. NW dynamics under 0.2-mT excitation of the 11.9-GHz mode in the ideal case.



VIDEO 2. NW dynamics under 0.2-mT excitation of the 16.3-GHz mode in the ideal case.



VIDEO 3. Spin-current injection ($J = 9 \times 10^{12}$ A/m²) in a 250-nm NW.



VIDEO 4. Transition from the BP-DW state to the SV state under the application of a 1-mT MW excitation field matching the frequency of the main SW mode in a 250-nm NW.

[1] M. Kammerer, M. Weigand, M. Curcic, M. Noske, M. Sproll, A. Vansteenkiste, B. Van Waeyenberge, H. Stoll, G. Woltersdorf, C. H. Back, and G. Schuetz, Magnetic vortex core reversal by excitation of spin waves, *Nat. Commun.* **2**, 279 (2011).
 [2] F. G. Aliev, J. F. Sierra, A. A. Awad, G. N. Kakazei, D. Han, S. Kim, V. Metlushko, B. Ilic, and K. Y. Guslienko,

- Spin waves in circular soft magnetic dots at the crossover between vortex and single domain state, *Phys. Rev. B* **79**, 174433 (2009).
- [3] A. A. Awad, K. Y. Guslienko, J. F. Sierra, G. N. Kakazei, V. Metlushko, and F. G. Aliev, Precise probing spin wave mode frequencies in the vortex state of circular magnetic dots, *Appl. Phys. Lett.* **96**, 012503 (2010).
- [4] F. G. Aliev, A. A. Awad, D. Dieleman, A. Lara, V. Metlushko, and K. Y. Guslienko, Localized domain-wall excitations in patterned magnetic dots probed by broadband ferromagnetic resonance, *Phys. Rev. B* **84**, 144406 (2011).
- [5] P. Chureemart, R. F. L. Evans, and R. W. Chantrell, Dynamics of domain wall driven by spin-transfer torque, *Phys. Rev. B* **83**, 184416 (2011).
- [6] R. Kohno, J. Sampaio, S. Rohart, and A. Thiaville, Domain wall propagation by spin-orbit torques in in-plane magnetized systems, *Phys. Rev. B* **102**, 020410 (2020).
- [7] Z. Sun, P. Fang, X. Shi, X. S. Wang, and F. Li, Field-driven side-by-side magnetic domain wall dynamics in ferromagnetic nanostrips, *Phys. Rev. B* **106**, 014412 (2022).
- [8] D. W. Wong, I. Purnama, G. J. Lim, W. L. Gan, C. Mura-paka, and W. S. Lew, Current-induced three-dimensional domain wall propagation in cylindrical NiFe nanowires, *J. Appl. Phys.* **119**, 153902 (2016).
- [9] R. Wieser, E. Y. Vedmedenko, P. Weinberger, and R. Wiesendanger, Current-driven domain wall motion in cylindrical nanowires, *Phys. Rev. B* **82**, 144430 (2010).
- [10] D. Raftrey, A. Hierro-Rodríguez, A. Fernández-Pacheco, and P. Fischer, The road to 3-dim nanomagnetism: Steep curves and architected crosswalks, *J. Magn. Magn. Mater.* **563**, 169899 (2022).
- [11] A. Fernández-Pacheco, R. Streubel, O. Fruchart, R. Hertel, P. Fischer, and R. P. Cowburn, Three-dimensional nanomagnetism, *Nat. Commun.* **8**, 15756 (2017).
- [12] K. Sobucki, M. Krawczyk, O. Tartakivska, and P. Graczyk, Magnon spectrum of Bloch hopfion beyond ferromagnetic resonance, *APL Mater.* **10**, 091103 (2022).
- [13] F. Zheng, F. N. Rybakov, A. B. Borisov, D. Song, S. Wang, Z. A. Li, H. Du, N. S. Kiselev, J. Caron, A. Kovács, and M. Tian, Experimental observation of chiral magnetic bobbars in B20-type FeGe, *Nat. Nanotechnol.* **13**, 451 (2018).
- [14] E. Feldtkeller, Mikromagnetisch stetige und unetige Magnetisierungskonfigurationen, *Z. Angew. Phys.* **19**, 530 (1965).
- [15] M. T. Birch, D. Cortés-Ortuño, N. D. Khanh, S. Seki, A. Štefančič, G. Balakrishnan, Y. Tokura, and P. D. Hatton, Bloch point-mediated skyrmion annihilation in three dimensions (2020), (unpublished).
- [16] D. Raftrey and P. Fischer, Field-Driven Dynamics of Magnetic Hopfions, *Phys. Rev. Lett.* **127**, 257201 (2021).
- [17] F. Tejo, R. Hernández Heredero, O. Chubykalo-Fesenko, and K. Y. Guslienko, The Bloch point 3D topological charge induced by the magnetostatic interaction, *Sci. Rep.* **11**, 21714 (2021).
- [18] O. Dmytriiev, U. A. S. Al-Jarah, P. Gangmei, V. V. Kruglyak, and R. J. Hicken, Static and dynamic magnetic properties of densely packed magnetic nanowire arrays, *Phys. Rev. B* **87**, 174429 (2013).
- [19] Y. Ivanov, A. Chuvilin, L. G. Vivas, J. Kosel, O. Chubykalo-Fesenko, and M. Vázquez, Single crystalline cylindrical nanowires—toward dense 3D arrays of magnetic vortices, *Sci. Rep.* **6**, 23844 (2016).
- [20] Y. Ivanov, M. Vázquez, and O. Chubykalo-Fesenko, Magnetic reversal modes in cylindrical nanowires, *Appl. Phys.* **46**, 485001 (2013).
- [21] I. M. Andersen, L. A. Rodríguez, C. Bran, C. Marcelot, S. Joulie, T. Hungria, M. Vazquez, C. Gatel, and E. Snoeck, Exotic transverse-vortex magnetic configurations in CoNi nanowires, *ACS Nano* **14**, 1399 (2020).
- [22] S. S. P. Parkin, H. Masamitsu, and L. Thomas, Magnetic domain-wall racetrack memory, *Science* **320**, 5873 (2008).
- [23] S. Ruiz-Gómez, M. Foerster, L. Aballe, M. P. Proenca, I. Lucas, J. L. Prieto, A. Mascaraque, J. de la Figuera, A. Quesada, and L. Pérez, Observation of a topologically protected state in a magnetic domain wall stabilized by a ferromagnetic chemical barrier, *Sci. Rep.* **8**, 16695 (2018).
- [24] J. A. Fernández-Roldán, R. Pérez del Real, C. Bran, M. Vazquez, and O. Chubykalo-Fesenko, Magnetization pinning in modulated nanowires: From topological protection to the “corkscrew” mechanism, *Nanoscale* **10**, 5923 (2018).
- [25] N. D. Mermin, The topological theory of defects in ordered media, *Rev. Mod. Phys.* **51**, 591 (1979).
- [26] E. Berganza, C. Bran, M. Jaafar, M. Vázquez, and A. Asenjo, Domain wall pinning in FeCoCu bamboo-like nanowires, *Sci. Rep.* **6**, 29702 (2016).
- [27] G. Sáez, E. Saavedra, N. Vidal-Silva, J. Escrig, and E. E. Vogel, Dynamic susceptibility of a Bloch point singularity confined in a magnetic nanowire, *Results Phys.* **37**, 105530 (2022).
- [28] E. Grimaldi, V. Krizakova, G. Sala, F. Yasin, S. Couet, G. Sankar Kar, K. Garello, and P. Gambardella, Single-shot dynamics of spin-orbit torque and spin transfer torque switching in three-terminal magnetic tunnel junctions, *Nat. Nanotechnol.* **15**, 111 (2020).
- [29] A. Vansteenkiste, J. Leliaert, M. Dvornik, M. Helsen, F. García-Sánchez, and B. Van Waeyenberge, The design and verification of MuMax3, *AIP Adv.* **4**, 107133 (2014).
- [30] J. P. Park, P. Eames, D. M. Engebretson, J. Berezovsky, and P. A. Crowell, Single-shot dynamics of spin-orbit torque and spin transfer torque switching in three-terminal magnetic tunnel junctions, *Phys. Rev. B* **67**, 020403 (2003).
- [31] M. P. Proenca, J. Rial, J. P. Araujo, and C. T. Sousa, Magnetic reversal modes in cylindrical nanostructures: From disks to wires, *Sci. Rep.* **11**, 10100 (2021).
- [32] A. Thiaville, J. M. García, R. Dittrich, J. Miltat, and T. Schrefl, Micromagnetic study of Bloch-point-mediated vortex core reversal, *Phys. Rev. B* **67**, 094410 (2003).
- [33] A. A. Thiele, Steady-State Motion of Magnetic Domains, *Phys. Rev. Lett.* **30**, 230 (1973).
- [34] K. Y. Guslienko, Gauge and emergent electromagnetic fields for moving magnetic topological solitons, *EPL* **113**, 67002 (2016).
- [35] R. Saha, Y. P. Pundir, and P. K. Pal, Comparative analysis of STT and SOT based MRAMs for last level caches, *J. Magn. Magn. Mater.* **551**, 169161 (2022).